

Wavelet characterisation of ionospheric acoustic and gravity waves occurring during the solar eclipse of August 11, 1999

P. Šauli^{a,*}, P. Abry^b, J. Boška^a, L. Duchayne^b

^a*Institute of Atmospheric Physics ASCR, Boční, 11/1401, Prague 4, 14131 Czech Republic*

^b*Laboratoire de Physique (UMR5672), CNRS, Ecole Normale Supérieure, Lyon, France*

Available online 28 October 2005

Abstract

We propose here a wavelet-based detection and characterisation of the propagation of acoustic-gravity waves induced in the ionosphere by the solar eclipse of August 11, 1999. The data are obtained from measurements of electron density profiles using (1 min vertical incidence) ionospheric sounding performed at Pruhonice (Czech Republic, 49.9N, 14.5E) and consist of the fluctuations of electron concentrations. The main goals of the current work are twofold. First, we describe in details the wavelet-based methodology used to detect and characterise acoustic and gravity waves and explain how and why this improves the previously proposed Fourier based approaches. Mainly, we show that wavelet transforms allow us to untangle waves that would be otherwise mixed up in Fourier decompositions. Second, we study carefully different waves and characterise them in terms of time of occurrence, period, wave vector, packet and phase velocities. We also demonstrate the existence of acoustic waves during the solar eclipse and characterise accurately. Such detections are made possible by the combined use of both data with a high sampling rate (1 min) and wavelet-based tools.

© 2005 Elsevier Ltd. All rights reserved.

Keywords: Solar eclipse; Acoustic-gravity waves; Vertical ionospheric sounding; Wavelet decomposition; Wave packet characterisation

1. Introduction

Because solar eclipses are rare events, the regular ionospheric effects of solar eclipses are still not well understood. Within a much shorter range of time much shorter than the usual day–night period, the ionosphere reconfigures itself into a state similar to that of a night-time situation, the photochemical activity decreases almost to night-time levels and then increases back to daytime value. The solar flux

first rapidly decreases, causing a cooling of the atmosphere at all heights and cessation of the ionization processes at ionospheric heights, and then increases yielding heating and return to a standard day state. Solar eclipses also induce significant changes in reflection heights, reductions in electron concentration in the F-layer maximum, increases of the F layer maximum height, and decreases in total electron content in the ionosphere. Such effects are usually characteristic of a night-time ionosphere. However, the movement of the eclipsed region at supersonic speed clearly differs from that of regular solar terminators at sunrise and sunset times.

These solar eclipse induced changes in the neutral atmosphere and ionosphere force the evolution of

*Corresponding author. Tel.: +420 272016067;
fax: +420 272763745.

E-mail addresses: pkn@ufa.cas.cz (P. Šauli),
Patrice.Abry@ens-lyon.fr, perso@ens-lyon.fr (P. Abry).

the ionospheric plasma toward a new equilibrium state. The return to equilibrium is likely to accompany eclipse induced wave motions excited in the neutral atmosphere that could cause significant variations in the electron and ion densities. These electron concentration oscillations, which depart from the standard solar controlled patterns, constitute the central material of the present analysis. However, in many cases, signatures induced by solar eclipses can easily be confused with some background fluctuations that may be due to geomagnetic activity, sporadic Es layer occurrence etc. Travelling ionospheric disturbances (TIDs) of auroral origin, for instance, can very well mask the disturbances produced by solar eclipse. Therefore, an important challenge consists in processing the data and in analysing the empirical time series to extract physical information (mainly detect the occurrence of acoustic gravity waves and characterise their propagations).

The disturbances induced by solar eclipses provide us with rare and exceptional natural *experiments* that enable us to study and understand dynamical processes, mechanisms and wave propagations at work in the ionosphere.

These effects are studied via ionospheric sounding techniques (GPS measurements, Radar techniques, Vertical ionospheric sounding etc.). Because the occurrences of solar eclipses can accurately be predicted, we are able to prepare campaigns of high sampling rate sounding of the ionosphere that enable us to collect high precision data.

The aim of the present work is to study dynamic processes during solar eclipse event which are associated with wave motions produced in the region of local temperature and ionization changes of the atmosphere as the Moon's shadow is advancing at a supersonic speed. The primary goal consists in proposing a thorough analysis of the acoustic and gravity waves that developed in the ionosphere during and just after the solar eclipse of August, the 11th, 1999. The data under analysis consists of the fluctuations in time (1 min sampling period) of electron concentrations at 21 different heights, ranging from 155 to 255 km (with a 5 km step). We introduce a wavelet-based methodology that enables, first, to detect waves amongst the background fluctuations, second, to accurately characterise these waves in terms of period, occurrence time, wave vector, packet and phase velocities. We argue that these wavelet approaches extend the Fourier based approach proposed earlier

(Liu et al., 1998; Altadill et al., 2001a) insofar as it avoids the mixing up of different waves. Being better separated, the waves are more relevantly studied and characterised. Besides gravity waves that are known to occur during and after the solar eclipse (Liu et al., 1998; Altadill et al., 2001a), we provide evidence for the existence of acoustic waves during the solar eclipse. We also characterise accurately and precisely these waves. To our knowledge, this is the first time that acoustic waves in solar eclipses are identified in experimental vertical incidence ionospheric measurements. We may emphasise the fact that this has been made possible by the use of a high repetition rate (1 min) sounding measurements together with a wavelet-based analysis.

Section 2 presents material on the solar eclipse of August 11, 1999 (parameters, measurements, analysed data and general physics). Section 3 introduces the wavelet transforms and defines the detection and characterisation methodology we developed. Sections 4 and 5 present the obtained results, comments and interpretations, respectively.

2. August 11, 1999 solar eclipse: physics, parameters, measurements and data

2.1. Parameters

The eclipse of August 11, 1999 was characterised by a low geomagnetic activity (Dst index varied from -10 nT to -20 nT, ΣK_p index reached the value of 12+). During the month of August 1999, Solar Flux was exceptionally quiet ($F_{10.7} = 128$). The central line duration of total eclipse was 2 min 20 s and the width of totality footprint was 110 km. Over the Pruhonice observatory, the first contact, the maximum and the fourth contact occurred respectively at 9 h 21.5 min UT, 10 h 42.4 min UT and 12 h 3.8 min UT. The Moon shadow velocity was of the order of 700 m s^{-1} over central Europe. The culmination of the solar eclipse over central Europe occurred at local noon, hence effects are well pronounced. This solar eclipse is notably exceptional in that it occurred during uniform solar disk, steady solar wind and quiet magnetospheric conditions. Hence, fluctuations in the ionosphere mainly consist of the signatures of the ionospheric responses to the solar eclipse. Detailed information about the solar eclipse can be found in the NASA database (<http://sunearth.gsfc.nasa.gov/eclipse/eclipse.html>).

2.2. Ionospheric measurements

Data were collected via a standard vertical incidence ionospheric sounding campaign, conducted at Pruhonice observatory (Czech Republic, 49.9N, 14.5E), using the classical ionosonde IPS 42 KEL Aerospace. These measurements are of high quality insofar as they are performed with an exceptionally short repetition time: 1 min. The corresponding ionograms have been scaled manually and the true-height electron density profiles were computed using the POLAN (POLynomial ANalysis) method (cf. Titheridge, 1985). During the eclipse event (during the recovery phase), the sporadic Es layer occurred, which complicated the scaling of several ionograms.

2.3. Data

The time series consist of the fluctuations of the electron concentrations at fixed heights z derived from true-height density profiles. Though we obtained electron density profiles from the bottom of E layer, we restrict our study to the region ranging from 155 to 255 km in order to avoid

complications due to a valley effect between E and F layers. The upper limit of the computation is chosen so as to satisfy the conditions of validity for the study of the variations and wave bursts in the electron concentration below the F2 layer peak.

We represent the data under analysis by:

$$X(t, z), \quad t \in [T_m, T_M], \quad z \in \mathbb{Z}. \quad (1)$$

Here, we have $\mathbb{Z} = \{155, 160, 165, \dots, 255\}$ (in km), $T_m = 08 \text{ h } 35 \text{ min}$, $T_M = 14 \text{ h } 20 \text{ min UT}$ and the time sampling period is $T_e = 1 \text{ min}$. The time series are plotted in Fig. 1.

2.4. Solar eclipse

In the localized eclipsed region, significant changes in the atmosphere and ionosphere are visible. The reduction in temperature causes a decrease of pressure over the totality footprint, which, in turn, induces a response of the neutral wind. A downwelling, downward transport of gas, results from the convergence of horizontal winds surrounding the eclipsed region. This causes a downward flux relative to pressure levels in order to ensure mass conservation. Downwelling upsets

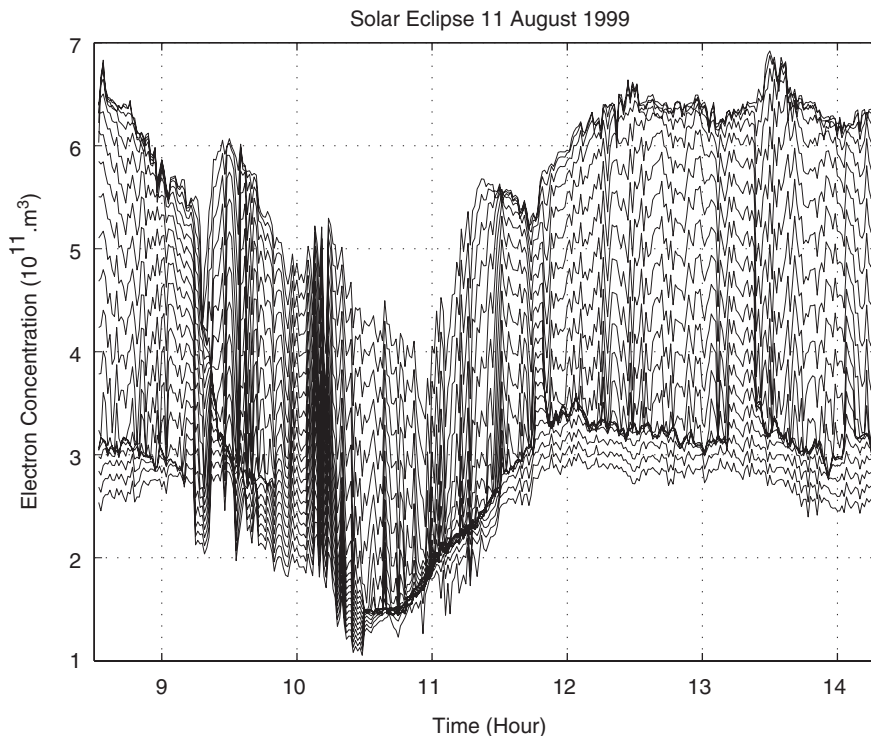


Fig. 1. *Fluctuations of the electron concentrations*: Empirical data to analyse consist of the fluctuations along time (1 min sampling period) of the electron concentrations at 21 different heights: $155 \leq z \leq 255 \text{ km}$ with a 5 km step.

the diffusive balance, so that the molecular diffusion reacts to restore the equilibrium. Cooling, downwelling and molecular diffusion are hence combined together (see e.g., Rishbeth et al., 1969; Muller-Wodarg et al., 1998).

As predicted in Muller-Wodarg et al. (1998), at the start of the solar eclipse the critical frequency of the F2 layer, foF2, undergoes a short increase followed by a decrease till its minimum that corresponds to the maximum solar disk occultation. E-layer reacts instantaneously to the decrease of the solar radiation flux due to photochemical processes and hence the Critical frequency foE decreases rapidly from about 3.5 MHz down to 2 MHz.

Fig. 1 shows the electron densities behavior in the F region height in 1 min sounding campaign. Electron concentrations vary first significantly and second differently during the initial and recovery phases of the Solar Eclipse. At all heights, the dominant trend consists first of a decrease during the solar disc occultation and cooling of the atmosphere (from about 9 UT till 11 UT) and second of a somehow faster increase (about 11 UT till 13 UT) during the recovery phase. Besides those main trends, strong wave-like oscillations are visible during all the solar eclipse. In the remainder of the present work, we concentrate on the detection, analysis and characterisation of these fluctuations. Our aim is to study to what extent they can be described in terms of acoustic or gravity waves (cf. Hines, 1960; Hooke, 1968).

2.5. Acoustic-gravity waves

We suppose that some of the wave bursts observed in the electron concentration variations (cf. Fig. 1) constitute the signature of acoustic-gravity waves that may have been produced in the neutral atmosphere and coupled into ionosphere or generated in situ within the ionospheric plasma. The propagation of the acoustic-gravity waves in the ionosphere as well as the coupling between neutral and ionised atmospheres have been studied at length by Hines (1960) and Hooke (1968). One proposed mechanism for the generation of acoustic-gravity waves during solar eclipse in the neutral atmosphere can be sketched as follows. The motion of the Moon's shadow, through the Earth's atmosphere at supersonic speed, screens the solar radiation producing an effective cooling spot. The absorption of ultraviolet radiation by ozone, that heats the middle atmosphere (effective maximum around 45 km), is

cut-off in the shadow region. As proposed by Chimonas and Hines (1970), the corresponding cooling effect constitutes a potential generator of acoustic-gravity waves that are likely to propagate up to and through ionospheric heights. This wave generation and wave properties were further reported and documented in Fritz and Luo (1993), Mims and Mims (1993) and Agashe and Rathi (1982) amongst others. However, those studies discussed gravity wave generation, mainly based on the assumption of solar eclipse heating effects on the ozone in the middle atmosphere. Another mechanism for wave generation was proposed in Muller-Wodarg et al. (1998). It combines effects of neutral atmosphere cooling and composition changes at ionospheric heights. Finally, at farther distances from the eclipsed region, the solar eclipse related ionospheric disturbances are mainly generated by the propagating bow shock (see e.g., Altadill et al., 2001a,b).

Most of the information related to the propagation of acoustic-gravity waves is contained in the corresponding dispersion relation Hines (1960):

$$\omega^4 - \omega^2 \omega_a^2 - k_x^2 C^2 (\omega^2 - \omega_g^2) - C^2 \omega^2 k_z^2 = 0, \quad (2)$$

where k_x and k_z stand for the horizontal and vertical components of the wave vector, C for the speed of sound, ω_a for the angular acoustic cut-off frequency and ω_g for the angular buoyancy (or Brunt–Väisälä) frequency. The propagation angle ϕ (measured from the vertical) in the atmosphere is defined by the ratio of the components of the wave vector:

$$\tan \phi = k_x / k_z. \quad (3)$$

This dispersion relation betrays a non linear and dispersive propagation and indicates that there exist two propagation ranges: acoustic modes, with frequencies larger than the acoustic cut-off ω_a , gravity modes, with frequencies smaller than the Brunt–Väisälä cut-off ω_g . To compute the parameters of the background neutral atmosphere at the studied heights, the Extended Australian Standard Atmosphere model 2000 (UASA2000) (Pietrobon, 2000) is used. It is the same as Standard Atmosphere 1976 model (USSA1976), except for the upper atmosphere, it is extended up to 1000 km. From this extension of the atmospheric parameters and using equations given in Davies (1990, p. 249), we were able to derive speed velocity, acoustic and Brunt–Väisälä cut-off frequencies as functions of z . Examples of computed parameters for the extreme

Table 1

Parameters of the neutral atmosphere (as computed from the Extended Australian Standard Atmosphere model 2000)

Height (km)	C (m s ⁻¹)	$2\pi/\omega_g$ (min)	$2\pi/\omega_a$ (min)
155	571.0	10.1	9.1
255	761.1	13.9	12.6

heights $z = 155$ km and $z = 255$ km are reported in Table 1.

3. Wavelet-based analysis

3.1. Wave packet description and Fourier decomposition

It has been proposed to describe waves in terms of wave packets:

$$X(z, t) = \int_{\omega_0(z)-\Delta\omega}^{\omega_0(z)+\Delta\omega} X_0(\omega, z) \exp i(\omega t - kz) d\omega, \quad (4)$$

where $X(z, t)$ stands for the amplitude of wave, $\omega_0(z)$ is the central frequency of the packet at altitude z and $\Delta\omega$ a characteristic frequency width of the wave packet. The methodology originally introduced in Liu et al. (1998) and further developed in Altadill et al. (2001a) proposed to derive the characteristic frequency, the z -components of the wave vector and the phase and packet velocities at all altitudes z from a Fourier analysis of the data $X(t, z) \rightarrow \hat{X}(\omega, z)$. We follow this original formulation and methodology but translate it into a wavelet framework. The goal is to obtain a joint time-frequency representation $T_X(\omega, t, z)$ of the wave packets to more accurately analyse them.

3.2. Wavelet transform

For a thorough introduction to wavelet transforms, the reader is referred e.g., to Mallat (1998). The wavelet transform of the data $X(t, z)$ is defined as:

$$T_X(a, t, z) = \int_{\mathbb{R}} X(u, z) \frac{1}{\sqrt{a}} \psi_0\left(\frac{u-t}{a}\right) du, \quad (5)$$

$a > 0, z \in \mathbb{Z},$

where $\psi_0(t)$ is a mother-wavelet. In the present work, we used Morlet and Paul (complex) mother-

wavelets, defined as:

$$\text{Morlet} : \psi_0(t) = (\pi\sigma^2)^{-1/4} \exp\left(-\frac{t^2}{2\sigma^2}\right) \exp(i2\pi\nu_0 t),$$

$$param = 2\pi\sigma\nu_0, \quad (6)$$

$$\text{Paul} : \psi_{0,N}(t) = \frac{2^N t^N N!}{\pi(2N)!} (1-t)^{-(N+1)},$$

$$param = N, \quad (7)$$

where $param$ counts roughly speaking the number of oscillations of the (real part) wavelet and provides the user with a degree of freedom that can be easily tuned to a given purpose. Because wave packets are usually analysed in terms of frequencies, pulsations or periods, we relabel, with a little abuse of notation, the wavelet coefficients $T_X(a, t, z) \equiv T_X(\omega, t, z)$ using the usual scale-frequency conversion: $\omega = \omega_\psi/a$, where ω_ψ is the central pulsation of the chosen mother-wavelet. It is straightforward to compute the ω_ψ s for the chosen mother-wavelets, as:

$$\omega_\psi = 2\pi \frac{\int_0^{+\infty} v |\Psi(v)|^2 dv}{\int_0^{+\infty} |\Psi(v)|^2 dv}, \quad (8)$$

where Ψ stands for the Fourier transform of ψ .

3.3. Scalograms

Because we choose to use complex mother-wavelet (Morlet and Paul), the wavelet coefficients $T_X(\omega, t, z)$ are complex numbers. Let $\{|T_X(\omega, t, z)|, \phi(\omega, t, z)\}$ denote their modulus and phase. Scalograms (also called wavelet power spectra) consist of (gray level) plots of $|T_X(\omega, t, z)|$ as a function of time t and period $P = 2\pi/\omega = 2\pi a/\omega_0$. Figs. 2 and 3 present some examples.

3.4. Wave packet detection and characterisation

The detection of wave packets consists in finding *significant* local maxima of the wavelet transform that exist *jointly* over different heights, almost with the *same time-period characteristics*, the corresponding characterisation is based on the phase of the wavelet transform. Let us describe more precisely the different steps of the detection-characterisation procedure we have developed.

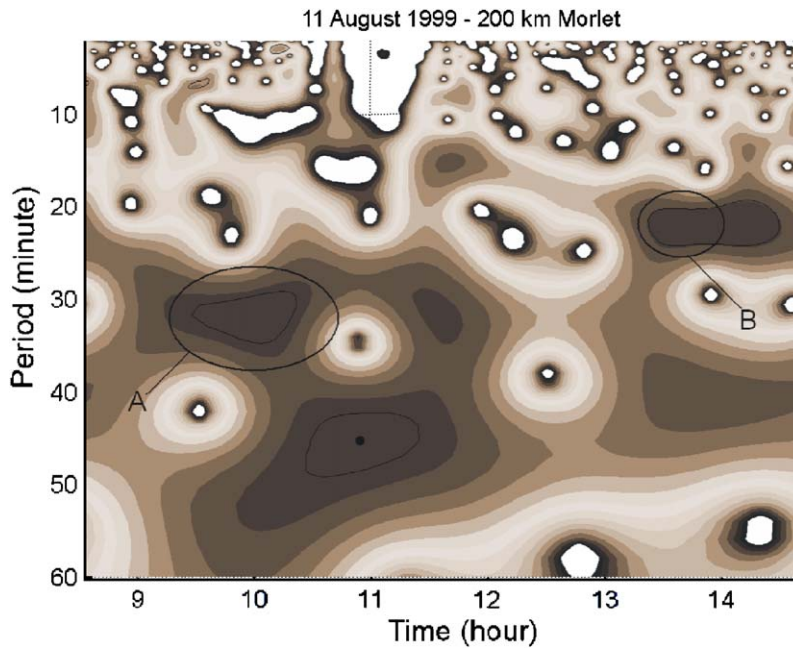


Fig. 2. *Scalogram*: This scalogram is computed using a Morlet mother-wavelet for $z = 200$ km and it studies periods ranging from 8 to 60 min. Amongst the numerous local maxima that can be observed only those that are found to coincide in time and period with local maxima over a significant range of heights z s and pass the dispersion relation consistency test correspond to the detection of wave structures. Two structures of particular interest, labelled A and B, are studied in detail.

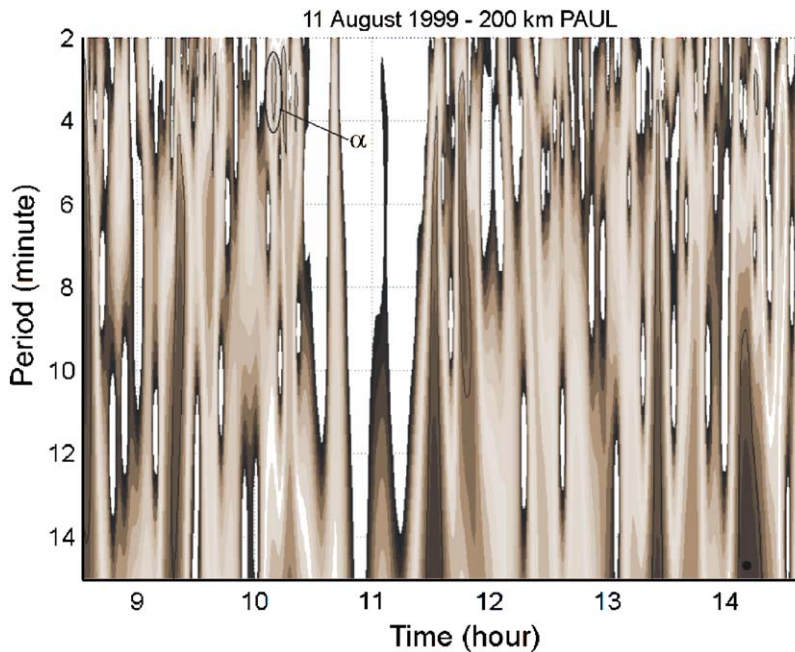


Fig. 3. *Scalogram*: This scalogram is computed using a Paul mother-wavelet for $z = 200$ km and concentrates on periods ranging from 2 to 15 min. Amongst the numerous local maxima that can be observed, one is found to coincide in time and period with local maxima over a significant range of z s and pass the dispersion relation consistency test. This structure, labelled α , is studied in detail.

- (i) For each z , high-pass filter each time series $\{X(t, z), t \in [T_m, T_M]\}_{z \in \mathbb{Z}}$ to suppress periods larger than 60 min. Compute the complex wavelet coefficients of the detrended data.
- (ii) For each z , locate maxima of the $|T_X(\omega, t, z)|$. When *significant* local maxima exist JOINTLY over a *continuous range* of heights z AND within a *same time-period neighbourhood*, we say that a wave packet (or wave or structure) is detected.
- (iii) Characterise each detection by its altitude range $z \in [z, \bar{z}]$, the precise time $t_0(z)$ and pulsation $\omega_0(z)$ of the occurrence of the maximum at each height z and the corresponding amplitude $X_0(z) = X(t_0(z), z)$. We also define the mean time and pulsation as:

$$\underline{t_0} = \langle t_0(z) \rangle_z, \quad \underline{\omega_0} = \langle \omega_0(z) \rangle_z, \quad (9)$$

where $\langle \cdot \rangle_z$ means that average is taken over the range of altitude $z \in [z, \bar{z}]$.

- (iv) Further characterise the wave packet through its wave vector, phase and packet velocities denoted by $k_0(z), v_{\phi,0}(z), v_{p,0}(z)$ and defined as:

$$\left. \begin{aligned} \text{Wave vector, } k_z(\omega, t, z) &= \frac{\partial \phi(\omega, t, z)}{\partial z}, \\ k_{0,z}(z) &= \langle \langle k(\omega, \underline{t_0}, z) \rangle \rangle_{\omega \sim \underline{\omega_0}}, \\ \text{Phase velocity, } v_\phi(\omega, t, z) &= \frac{\omega}{k(\omega, t, z)}, \\ v_{\phi,0}(z) &= \langle \langle v_\phi(\omega, \underline{t_0}, z) \rangle \rangle_{\omega \sim \underline{\omega_0}}, \\ \text{Packet velocity, } v_{p,z}(\omega, t, z) &= \frac{\partial \omega}{\partial k_z(\omega, t, z)}, \\ v_{p,0}(z) &= \langle \langle v_{p,z}(\omega, \underline{t_0}, z) \rangle \rangle_{\omega \sim \underline{\omega_0}}, \end{aligned} \right\} \quad (10)$$

where $\langle \langle \cdot \rangle \rangle_{\omega \sim \underline{\omega_0}}$ denote that we take the median over a narrow range of pulsations centred around $\underline{\omega_0}$. From ionospheric vertical sounding measurements, one only has access to vertical profiles of electron density and hence to the vertical components of the wave vector, phase and packet velocities. Therefore, all the quantities defined in Eq. (10) above stand for the vertical components of the corresponding vectors only.

- (v) For each detection/characterisation, perform a consistency check with the standard dispersion relation (cf. Eq. (2)). Using the extended UASA2000, we compute $C(z), \omega_g(z)$ and $\omega_a(z)$. From measurements, we have $w_0(z)$ and $k_{0,z}(z)$. As previously mentioned, there exist two propagation modes, acoustic waves with permitted periods below acoustic cut-off frequency and gravity waves, with permitted periods

above Brunt–Väisälä one. From a practical point of view, this means that we search for waves with frequencies in the corresponding ranges (practical numerical values were given in Table 1 above). Hence, we check that $w_0(z)$ does not fall within the forbidden range and classify the wave as acoustic or gravity. Using Eqs. (2) and (3), we compute $k_{0,x}(z)$ and $\tan |\phi|$, respectively. Then it is straightforward to derive $|v_{\phi,x}|$.

We adapted the wavelet decomposition Matlab codes provided by Torrence and Compo (cf. Torrence and Compo, 1998) to our purposes (Morlet and Paul mother-wavelets with parameters $param = 6$ and $param = 2$, respectively, were used).

4. Results

4.1. Scalograms: general comments

For each of the 21 different available heights, scalograms were computed with Morlet ($param = 6$) and Paul ($param = 2$) wavelets, for the entire observation times ($08 \text{ h } 35 \text{ min} \leq t \leq 14 \text{ h } 20 \text{ min}$) for periods ranging from 8 to 60 min and 2 to 15 min, respectively. The entire set of (the $21 \times 2 \times 2$) scalograms cannot be shown here. Three of them are presented in Figs. 2–4, with the arbitrary choice $z = 200 \text{ km}$. A thorough inspection of the whole set of scalograms yields the following comments.

For $z \leq 180 \text{ km}$, a large number of wave bursts can be observed before the maximum solar disc occultation (around $t \simeq 11 \text{ h}$). For $185 \leq z \leq 215 \text{ km}$, strong wave bursts can be observed during all the duration of the solar eclipse event and even after the end of solar disc occultation. Above 215 km, wave-like oscillations occur mainly during the initial phase of the solar eclipse. During the recovery phase, the wave activity is significantly weaker.

Amongst all the observed bursts, corresponding to local maxima in the time-period domain at given heights z , only those that are found to coincide in time and period over a significant range of heights are selected as potential wave-like patterns. Among this set, a number of candidates are ruled out as they do not pass the dispersion relation consistency check mentioned above. Several structures that possess the properties of acoustic-gravity waves as per theory were detected.

Three of them are chosen for a detailed analysis reported below. Structures A and B (cf. Fig. 2) correspond to waves taking place during and after the eclipse with characteristic periods about 23 and 28 min, respectively. Structure α (cf. Fig. 3) corresponds to a wave taking place during the eclipse with a characteristic period about 4 min.

4.2. The wavelet contribution: illustrations on an example

To highlight the role of the wavelet decomposition, let us have a close look at Structure α . Fig. 4 consists of a zoom of the scalogram shown in Fig. 3 within the subrange $t \in [10\text{ h }00, 10\text{ h }50\text{ min}]$ and $P \in [2, 4.6]\text{ min}$. It shows that there exist two other waves occurring just after Structure α . By construction, a Fourier based analysis would mix up those structures and would not enable us separate them. The wavelet transform, because it benefits from an optimal time and frequency joint resolution, enables us to clearly untangle these different structures and to study them independently and hence to accurately characterise them. Indeed, trying to charac-

terise α without distinguishing those different structures would yield an incorrect characterisation while studying each of them independently leads to a correct analysis. This is where the wavelet approach brings a clear benefit compared to the Fourier one. Below, we studied in detail the structure occurring between 10 h 06 min and 10 h 15 min. Paul wavelet, because it benefits from a better time resolution compared to Morlet wavelet, proved experimentally more useful to characterise waves.

4.3. Gravity waves

Fig. 5 presents the wavelet-based characterisations of waves A and B selected in Fig. 2. Both of them correspond to gravity waves. Indeed, the fact that their vertical components of the phase and packet velocities have opposite signs constitutes a standard signature of gravity waves, in consistence with the dispersion relation.

Wave A occurs around $t_0 = 9\text{ h }25\text{ min}$ (i.e., during the solar eclipse) and with characteristic period $P_0 \simeq 23\text{ min}$. As indicated by the sign of the

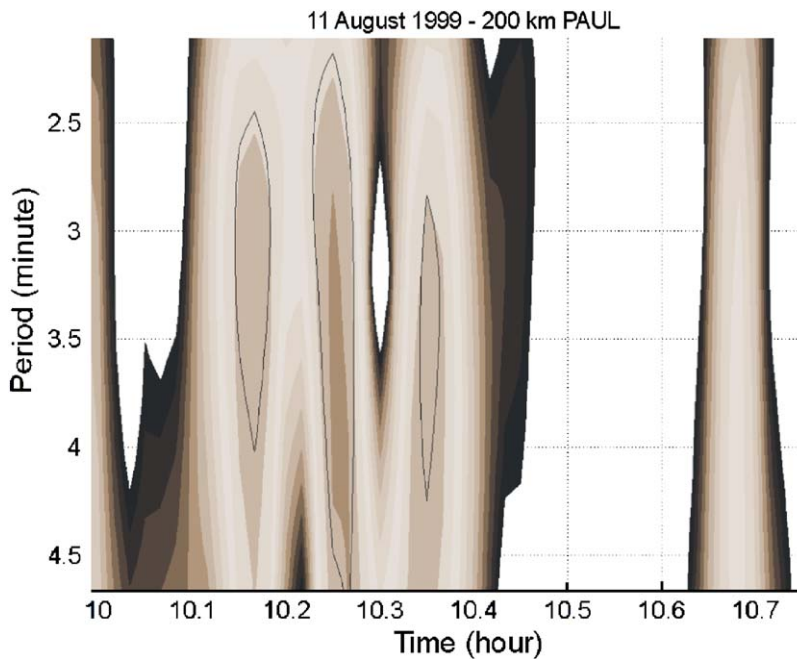


Fig. 4. *Zoom in scalogram*: This scalogram is a zoom of the one in Fig. 3, in the range $2 \leq P \leq 4.6\text{ min}$ and $10\text{ h }00\text{ min} \leq t \leq 10\text{ h }15\text{ min}$. It shows that three different local maxima occur one after the other in the same time-period neighbourhood. A Fourier based approach would not enable us to separate them while the wavelet based one clearly does. It allows us to characterise them independently and hence correctly while a characterisation that would not separate them would yield irrelevant results. In the text, we study in detail the first of these three maxima, labelled α (i.e., $10.1 \leq t \leq 10.2$), as it is coinciding in time and period with other local maxima over a continuous range of z s.

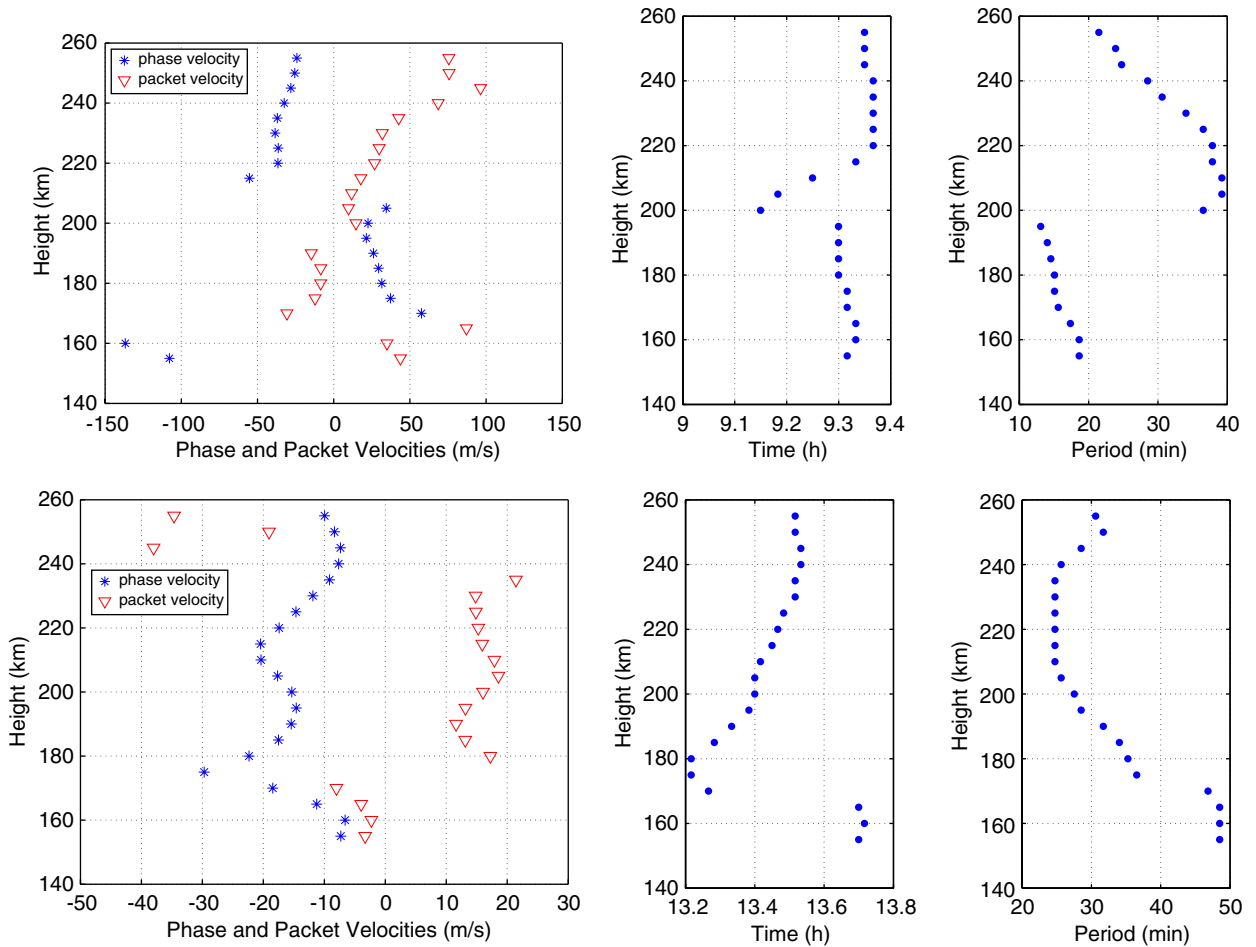


Fig. 5. Gravity waves characterisation: Waves A and B (top and bottom respectively) in Fig. 2 correspond to gravity waves. Left plot, z -component of the packet an phase velocities (in m s^{-1}), middle plot, wave occurrence time (in hours), right plot, propagating period (in min), as a function of heights z . The direction of the energy flow is indicated by the sign of the packet velocity. Wave A occurs around $t_0 = 9 \text{ h } 25 \text{ min}$ (within the solar eclipse), with $P_0 \simeq 23 \text{ min}$, it can be clearly seen that its origin is located around $z = 210 \text{ km}$ and that it propagates upward and downward from this source region. Wave B occurs around $t_0 = 13 \text{ h } 25 \text{ min}$ (after the solar eclipse), with $P_0 \simeq 28 \text{ min}$. It propagates upward in the range $175 \leq z \leq 235$.

Table 2
Gravity (A and B) and acoustic (α) waves characterisation

Type Wave	Gravity A	Gravity A	Gravity B	Gravity B	Acoustic α	Acoustic α
Height (km)	175	230	175	230	175	230
Period (min)	15	33	37	25	4.4	3.5
$v_{\phi,z}$ (m s^{-1})	48	-52	-30	-14	-768	965
$ v_{\phi,x} $ (m s^{-1})	42.4	116.7	95.7	22	1528	1205
$ \phi $	48.5°	156.0°	162.6°	147.0°	153.0°	38.7°

packet velocity, the (energy of the) wave propagates upward for $z \geq 215$ and downward for $z \leq 195$. As shown on middle plot, the wave packets

propagate simultaneously upward and downward from mid-heights but with slightly different periods. It can also be clearly seen that its origin is located around $195 \leq z \leq 215 \text{ km}$. Table 2 summarises its characteristics.

Wave B corresponds to a wave that develops in the range $175 \leq z \leq 235$ (as can be seen in Fig. 5, bottom plots). Its positive packet velocity shows that the (energy of the) wave propagates upward. It occurs around $t_0 = 13 \text{ h } 25 \text{ min}$, hence after the solar eclipse and one can notice that its period is decreasing from 35 to 25 min while propagating upward. The sporadic Es layer happens to be present in several ionograms at these times. This

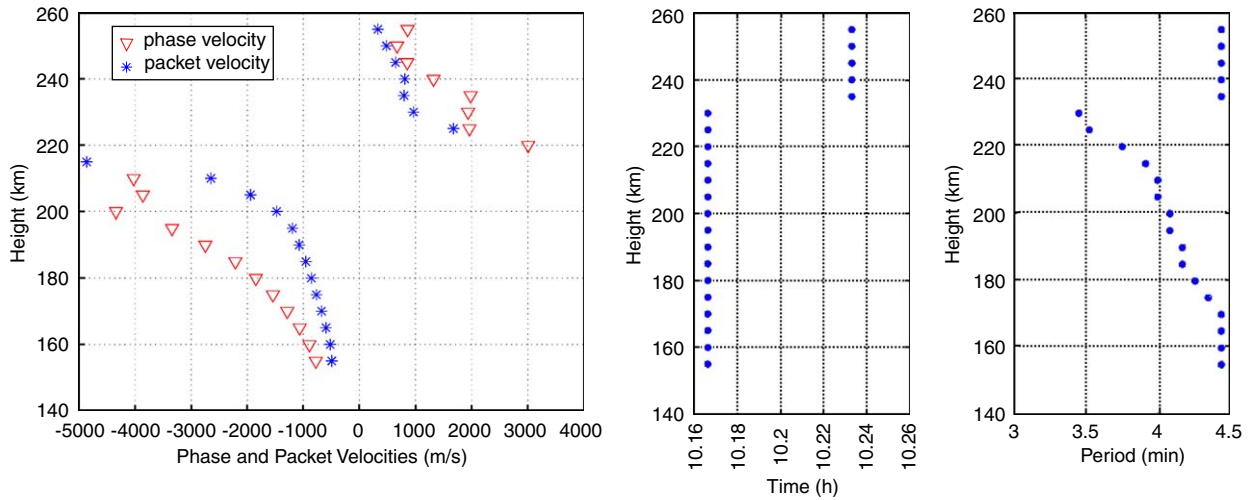


Fig. 6. *Acoustic waves characterisation*: Waves α in Fig. 3 correspond to Acoustic waves. Left plot, z -component of the packet and phase velocities (in m s^{-1}), middle plot, wave occurrence time (in hours), right plot, propagating period (in min), as a function of heights z . The direction of the energy flow is indicated by the sign of the packet velocity. Both waves are located within the solar eclipse. Wave α occurs around $t_0 = 10 \text{ h } 15 \text{ min}$, with $P_0 \simeq 4 \text{ min}$, it can be clearly seen that its origin is located around $z = 230 \text{ km}$ and that it propagates upward and downward from this source region.

may slightly affect the derivation of the characteristics of structure B and is likely responsible for the discrepancy observed at heights below 175 km.

4.4. Acoustic waves

Fig. 6 shows the wavelet-based properties of waves α selected from the scalogram (cf. Fig. 3). The phase and packet velocity vertical components have identical signs, a necessary property of acoustic waves (cf. dispersion relation in Eq. (2)). Both chosen structures occur during the solar eclipse. Their notably constant occurrence times as a function of z betrays a significantly high z -component of the packet velocities, in consistence with the dispersion relation.

Structure α takes place around $t_0 = 10 \text{ h } 15 \text{ min}$ with $P_0 \simeq 4 \text{ min}$. In the range of heights $z \geq 235$, the wave propagates upward, while at heights $z \leq 230$, the wave is moving downward. Apparently, the wave packets propagate simultaneously upward and downward from the region round 230 km.

5. Discussion and interpretation

We studied several wave structures, that can mainly be classified in terms of nature (gravity or acoustics), and/or of time of occurrence (within or after the solar eclipse) and/or source region (within the ionosphere or in the neutral atmosphere below).

5.1. Source region

Waves A and α provide us with examples of in situ gravity and acoustic wave generation in the ionospheric plasma because they share the important property that their source regions are located within the ionosphere, at heights close to 200 km. This region coincides with the border between F1 and F2 regions. The transition height, where the density of O^+ (characteristic for F2 region) is equal to the molecular ion density (dominant in F1 region), typically occurs at height 180 km. In the F1 region, all photochemical reactions are fast compare to those taking place in F2 region. The electron density in F1 region immediately decreases with the solar disc occultation and temporary reduction in the ionization radiation. The F2 layer responds with a short delay. In the F2 layer, the electron concentration increases at heights close to F2 peak (the value of foF2 rises for about 30 min), this is caused by the atmosphere's compression and then decrease (cf. Muller-Wodarg et al., 1998). Therefore, differences between F1 and F2 regions in the response to the radiation flux changes are responsible for sharp gradients electron and ion concentrations arising from the faster depletion of the region F1 compared to region F2. This area is located around 200 km and likely act as an acoustic-gravity wave generator. Similar mechanism of wave generation was proposed by (Somsikov, 1991), narrow region of sharp

gradients of temperature, pressure and electron and ion concentrations between two states of the atmosphere corresponding to the night and day conditions launched gravity waves at sunrise and sunset hours. Furthermore, the acoustic and gravity waves propagate simultaneously upward and downward from the source region.

Wave B propagates upward through the whole ionosphere and seems to be originated from below the studied heights. This example of propagating wave can be attributed to the movement of the cooled spot produced by the moon's shadow in the ozone layer at heights around 45 km. This wave generation mechanism, proposed in Chimonas and Hines (1970) and further studied in Fritz and Luo (1993), is a consequence of the interruption of the ozone heating. Such produced waves can propagate upward up to ionospheric heights and may have an important dynamical influence there.

5.2. Occurrence time

Waves A and α occur during the solar eclipse while wave B takes place in the recovery phase. Hence, we were able to find evidence for the existence of gravity waves both during and after the eclipse, while we found clear evidences of acoustic waves within the eclipse only. Despite efforts in search for acoustic waves taking place after the maximum solar disk occultation, we found valid acoustic waves propagating in narrow ranges of heights only. The presence of the sporadic Es layer in several ionograms may cause inaccuracies in scaling and subsequently affects the final profile of electron concentration. This significantly impairs a relevant characterisation of the waves. Acoustic waves, with periods of a few minutes, are likely to be more sensitive than gravity waves to possible inaccuracies in the available data. Our methodology also requires further improvements to deal with waves propagating in a narrow range of heights. Hence, further studies are necessary to conclude whether acoustic waves propagate or not through the ionospheric heights during recovery phase and after eclipse.

5.3. AGW and solar eclipse

Acoustic and gravity waves (AGW) exist in ionosphere even when there is no solar eclipse. Many works reported occurrence of AGW in ionosphere, studied them in details and related

them to various possible sources. To decide whether the waves detected in the present work are to be associated to the solar eclipse or not, one should ideally perform direct comparisons against waves detected during regular days in the same context and with the same data acquisition and analysis methodologies. However, such ideal comparisons cannot be simply performed due to the lack of the corresponding measurements. Comparisons can be drawn against studies of 5-min ionospheric sounding, such as those in Altadill et al. (1999), Boška and Šauli (2001), Boška et al. (2003), Martinis and Manzano (1999), Šauli and Boška (2001) and Šauli et al. (2005), satellite or rocket measurements such as Bertin et al. (1978) and Kelley (1997), arrays of ionosonds as reported in Somsikov (1991) and many others. We can compare the times of occurrence, differences and similarities in the vertical structure and source location. According to the vertical components of propagation, waves occurring in the ionosphere except for sunrise and sunset periods, can be classified into two groups. Waves with significant vertical component of movement that propagate from lower layers of the atmosphere and might have their origin in, for instance, meteorological phenomena etc., and waves with very small vertical component of movement that propagate horizontally from auroral region and that are related to the geomagnetic disturbances. Works by Somsikov (1991), Boška et al. (2003) and Šauli et al. (2005) reported regular occurrence of gravity waves during morning and evening hours that are likely to be produced by solar terminator movements. Such waves remain within ionosphere only for a short time period during sunrise and sunset hours and have characteristics similar to the waves detected in the present work in terms of source region location (round 200 km) and propagations upward and downward from this region. It is natural to imagine that a similar mechanism can be involved in the production of waves during solar eclipse and sunrise and sunset waves (Chimonas and Hines, 1970; Somsikov, 1990). We suppose that, since the solar eclipse occur sufficiently after sunrise, the detected waves cannot be mixed with morning solar terminator waves. Since the detected waves propagate upward and downward from the source region as solar terminator induced waves we suppose that they can be attributed to the atmospheric cooling and heating during solar eclipse. All these reasons lead us to strongly believe that the detected AGW are induced by the solar eclipse.

6. Conclusion

The two major results of the present work consist of the development of a wavelet-based methodology to detect and characterise propagating waves and in the fact that we evidenced the existence of acoustic waves and characterised them.

We studied in details acoustic and gravity waves and showed that their derived propagation characteristics are in agreement with the theoretical predictions. Our study seems to suggest also two different possible source region locations: F1/F2 transition and abruptness of ozone heating in the middle atmosphere.

The detection of acoustic waves, which is a non straightforward experimental result, was made possible because we used high time resolution (1 min sampling period) measurements jointly with a wavelet analysis instead of a Fourier one. We showed that the use of this joint time-frequency representation of the data enables to identify and locate (and therefore characterise) waves in a more accurate way than the Fourier based analysis would do and to untangle possibly mixed up waves and structures.

At this stage, the detection procedure remains manual and still requires careful human inspection and supervision, and so do the characterisation steps. The proposed methodology hence requires further improvements to be made automatic and less supervised. This is under current investigations.

Acknowledgements

This work has been supported by the Grant Agency of the Czech Republic, Grants No. 205/02/P077/A and No. 205/01/1071, Grant A3042102/012/01 of the Grant Agency of the Academy of Sciences of the Czech Republic. One of the author (PA) thanks IAP ASCR for its financial support during his visit at IAP in 2002 and 2003. The authors acknowledge the joint financial supports of Département des Sciences de la Matière, ENS Lyon and IAP, Praha, for Loic Duchayne long stay in Praha, during which the final stages of this work were accomplished. The authors thank two anonymous reviewers for their careful reading and accurate comments on the first draft of the paper. They also acknowledge the support of the Grant 18098 from the French CNRS and Czech ASCR enabling further developments for this project.

References

- Agashe, V., Rathi, S.M., 1982. Changes in the concentration of mesospheric ozone during the total solar eclipse. *Planetary and Space Science* 30, 507–513.
- Altadill, D., Boška, J., Solé, J.G., Alberca, L., 1999. Short-time fluctuations in the F region electron density, Proceedings COST 251 meeting, Madeira.
- Altadill, D., Gauthier, F., Vila, P., Sole, J.G., Miro, G., Berranger, R., 2001a. The 11.8.1999 solar eclipse and the ionosphere: a search for distant bow-wave. *Journal of Atmospheric and Solar-Terrestrial Physics* 63 (9), 925–930.
- Altadill, D., Sole, J.G., Apostolov, E.M., 2001b. Vertical structure of a gravity wave like oscillation in the ionosphere generated by the solar eclipse of August 11, 1999. *Journal of Geophysical Research—Space Physics* 106 (A10), 21419–21428.
- Bertin, F., Testud, J., Kersley, L., Rees, P.R., 1978. The meteorological jet stream as a source of medium scale gravity waves in the thermosphere: an experimental study. *Journal of Atmospheric and Solar-Terrestrial Physics* 40, 1161–1183.
- Boška, J., Šauli, P., 2001. Observations of gravity waves of meteorological origin in the F-region. *Physics and Chemistry of the Earth (C)* 26 (6), 425–428.
- Boška, J., Šauli, P., Altadill, D., Sole, J.G., Alberca, L., 2003. Diurnal variation of the gravity wave activity at midlatitudes of ionospheric F region. *Studia Geophysica & Geodetica* 47, 579–586.
- Chimonas, G., Hines, C.O., 1970. Atmospheric gravity waves induced by a solar eclipse. *Journal of Geophysical Research* 75 (4), 875.
- Davies, K., 1990. *Ionospheric Radio*. Peter Peregrinus Ltd., London, UK.
- Fritz, D.C., Luo, Z.G., 1993. Gravity-wave forcing in the middle atmosphere due to reduced ozone heating during a solar eclipse. *Journal of Geophysical Research* 98 (D2), 3011–3021.
- Hines, C.O., 1960. Internal atmospheric gravity waves at ionospheric heights. *Canadian Journal of Physics* 38, 1441–1481.
- Hooke, W.H., 1968. Ionospheric irregularities produced by internal atmospheric gravity waves. *Journal of Atmospheric and Solar-Terrestrial Physics* 30, 795–823.
- Kelley, M.C., 1997. In situ observations of severe weather-related gravity waves and associated small-scale plasma structures. *Journal Geophysical Research—Space Physics* 102, 329–335.
- Liu, J.Y., Hsiao, C.C., Tsai, L.C., Liu, C.H., Kuo, F.S., Lue, H.Y., Huang, C.M., 1998. Vertical phase and group velocities of internal gravity waves derived from ionograms during the solar eclipse of 24 October 1995. *Journal of Atmospheric and Solar-Terrestrial Physics* 60, 1679–1686.
- Mallat, S., 1998. *A Wavelet Tour of Signal Processing*. Academic Press, San Diego.
- Martinis, C.R., Manzano, J.R., 1999. The influence of active meteorological systems on the ionospheric F-region. *Annals of Geophysics* 42 (1), 1–7.
- Mims, F.M., Mims, E.R., 1993. Fluctuation in column ozone during the total solar eclipse of July 11, 1991. *Geophysical Research Letters* 20, 367–370.
- Muller-Wodarg, I.C.F., Aylward, A.D., Lockwood, M., 1998. Effects of a mid-latitude solar eclipse on the thermosphere and ionosphere—a modelling study. *Geophysical Research Letters* 25 (20), 3787–3790.

- NASA Database: <http://sunearth.gsfc.nasa.gov/eclipse/eclipse.html>
- Pietrobon, S.S., 2000. <http://www.sworld.com.au/steven/space/atmosphere/>
- Rishbeth, H., Moffett, R.J., Bailey, G.J., 1969. Continuity of air motion in the mid-latitude thermosphere. *Journal of Atmospheric and Solar-Terrestrial Physics* 31, 1035–1047.
- Šauli, P., Boška, J., 2001. Tropospheric events and possible related gravity wave activity effects on the ionosphere. *Journal of Atmospheric and Solar-Terrestrial Physics* 63, 945–950.
- Šauli, P., Abry, P., Altadill, D., Boška, J., 2005. Detection of the wave-like structures in the F-region electron density: two station measurements. *Sudia Geophysica and Geodetica*, in press.
- Somsikov, V.M., 1991. Waves in the atmosphere excited by the solar terminator. *Geomagnetism and Aeronomy* 31 (1) (in Russian).
- Titheridge, J.E., 1985. Ionogram analysis with the generalised program POLAN, UAG Report-93.
- Torrence, C., Compo, G.P., 1998. A Practical guide to wavelet analysis. *Bulletin of American Meteorological Society* 79 (1), 61–78.